https://dx.doi.org/10.21577/0103-5053.20220066

J. Braz. Chem. Soc., Vol. 33, No. 11, 1342-1351, 2022

Article

The Influence of the Platinum Weight Percentage in the Catalyst Formulation on the Performance of a High Temperature Ethanol Electroreformer Based on H_3PO_4-Doped Polybenzimidazole for Green Hydrogen Production

Bruno G. C. Alves,[a] Dryade F. de Paula,[a] Rudy Crisafully[a] and José J. Linares *,[a]*

[a]*Laboratório de Desenvolvimento de Processos Químicos, Instituto de Química, Universidade de Brasília, Campus Universitário Darcy Ribeiro, 70910-900 Brasília-DF, Brazil*

A vapor-fed high temperature proton exchange ethanol electroreformer has been developed based on the use of a H_3PO_4-doped polybenzimidazole membrane to produce green hydrogen. As a key parameter, this article describes the influence of platinum weight percent (wt.%) in the catalyst formulation from different commercial catalysts (20, 40, 60, 80 wt.% Pt/C and Pt black) on the activity (related to the H_2 production), energy consumption, and CO_2 yields. The structural and morphological analysis reveal that an increase in Pt wt.% leads to the formation of bigger nanometric Pt particles, resulting in a decrease in the electrochemically active surface area. In terms of the ethanol electro-oxidation activity, the Pt wt.% impacts on the performance of the electroreformer, with the H_2 flux that increase from 0.22 STP (standard pressure and temperature, 273.15 K and 105 Pa) $m^3\ m^{-2}\ h^{-1}$ for Pt black to 1.47 STP $m^3\ m^{-2}\ h^{-1}$ for 60 wt.% Pt/C. The Pt wt.% also impacts on the CO_2 percentages, increasing from values in the range of 20-40% for the 20 wt.% Pt/C to 45-55% for the optimum 60 wt.% Pt/C and, finally, decreasing to values between 30-45% for Pt black. These values are, in overall, higher than those of low temperature (< 90 °C) ethanol electro-oxidation systems.

Keywords: ethanol, electrolysis, hydrogen, CO_2, Pt/C, efficiency

Introduction

Hydrogen is receiving increased attention due to its crucial role as an energy vector in the progress towards substituting fossil energy sources for renewable energy sources (RES). Its importance derives from its versatility, which is exemplified by its ability to bridge the gap between the supply and demand of RES, through its generation/storage in electrolyzers during periods of excess supply, followed by its utilization in fuel cells to produce electricity during peaks of demand.[1] Nevertheless, the whole success of this principle relies on the development of technologies that permit the production of so-called "green hydrogen"-hydrogen generated from electrolysis powered by RES feedstocks.[2] Water electrolysis is the main and more mature representative, commercialized during the last century, stimulated particularly by the chloro-alkali industry.[3] The main issue that water electrolysis faces is the large energy consumption associated with the electromotive force (EMF = 1.23 V), which during operation can rise up to 1.6-1.8 V, owing to the large overvoltage of the oxygen evolution reaction.[4] This corresponds to an average electrical demand of approximately 55 kWh kg^{-1} of H_2.[5] To further reduce the costs of hydrogen (CoH), the International Renewable Energy Agency defined a goal of decreasing that energy demand by ca. 30%. This is one of the requirements for making green hydrogen competitive compared to fossil fuel-based hydrogen ("grey hydrogen").[5,6]

The replacement of water by alcohols at the anode is one of the alternative methods for reducing energy consumption, in the so-called alcohol electroreformers.[7] This technology reduced the CoH through a decrease in the EMF, as there is a lower standard redox potential for alcohol oxidation (0.0 to 0.1 V *vs.* normal hydrogen energy, NHE) compared to water oxidation (1.23 V *vs.* NHE).[8] Ethanol is one of the alcohols used for hydrogen production by electroreforming, displaying a reduced energy demand in proton exchange membrane electroreformers (PEME).[9-14] However, the use of conventional perfluorosulfonated PEM (proton exchange membranes) limits the operating temperature to 90 °C, resulting in reduced values of the faradaic efficiency of the ethanol electro-oxidation (EEO), owing to incomplete oxidation to acetaldehyde (16.7%) or acetic acid (33.3%),

*e-mail: joselinares@unb.br
Editor handled this article: Rodrigo A. A. Muñoz (Associate)

rather than the 12 e^- process of complete oxidation to CO_2.[15-20] An alternative strategy for increasing the efficiency of the EEO is to use an alternative PEM, so that the temperature can be increased to above 100 °C and overcome the energy barrier of C–C cleavage.[21,22]

Given this background, this study proposes to develop, for the first time, a high temperature ethanol PEME based on the utilization of a H_3PO_4-doped polybenzimidazole membrane (HT-PA-PBI-PEMEtE). With this, we intend to combine the production of green hydrogen with the maximization of the selectivity of the ethanol oxidation to CO_2 to increase the faradaic efficiency, thus overcoming this limitations of the low temperature ethanol PEME. For this first study, commercial Pt/C electrocatalysts with different Pt weight percent (wt.%) in their formulations have been used as the anode catalyst. Previous studies[23,24] based on measurements of H_2SO_4 as electrolyte in the three-electrode glass cell and Nafion®-based direct ethanol fuel cells (DEFC) demonstrated that such a parameter strongly influences the geometrical and electronic characteristics of the Pt nanoparticles, altering the reactivity of the reactants and intermediates, and the oxophilicity of the Pt surface-a crucial factor for the activity of the EEO. This parameter has been also explored for the methanol electro-oxidation,[25,26] and for the glycerol electro-oxidation,[27] influencing the electrochemical activity and, in the case of glycerol, the product distribution. Nevertheless, studies referred to the EEO in H_3PO_4 are relatively scarce,[21,22,28-32] and with the exception of the work presented by Lobato *et al*.,[32] in which they studied two different metallic loadings of a bimetallic PtRu (20 and 60 wt.% on carbon nanofibers), observing differences attributed to the different degree of alloying, there are no systematic studies in this environment analyzing the influence of this parameter on H_3PO_4 as electrolyte and, more interestingly, applied on a HT-PA-PBI-PEMEtE, aiming at producing green hydrogen with the lowest possible energy demand and with the maximum complete ethanol conversion to CO_2. The materials have been characterized by thermogravimetric analysis (TGA), X-ray diffraction (XRD) and transmission electron microscopy (TEM). Electrochemical studies have also been performed in a three-electrode cell to determine the activity towards the EEO and, finally, the catalysts have been applied to a HT-PA-PBI-PEMEtE. The electrochemical performance, hydrogen production and the relative distribution of the EEO products were monitored. To the authors' knowledge, this is the first report of such a type of device.

Experimental

Commercial Pt/C with different Pt wt.% (20, 40, 60, 80 wt.% on carbon black Vulcan XC-72R) and Pt black, were purchased from Novocell (Americana, SP, Brazil). These materials were characterized by TGA in a Shimadzu DTG-60H apparatus (Shimadzu Ltd, Kyoto, Japan) with a synthetic air flow of 20 mL min^{-1} applying a heating ramp of 10 °C min^{-1} from room temperature up to 900 °C. From the TGA, it is possible to estimate the Pt percentage based on the combustion of the carbon support to form CO_2. The remaining weight accounts for the Pt metal loading.[33-35] XRD analyses were carried out in a Bruker model D8 Focus diffractometer using Cu Kα radiation (Bruker λ = 0.15406 nm, Billerica, Massachusetts, USA). The diffractograms were recorded with 2θ angles in the range of 20-90° (0.05-degree step, 0.5 degree min^{-1}). Transmission micrographies were obtained from a JEOL 2100 microscope (Jeol do Brasil Ltda., São Paulo, SP, Brazil) at 200 kV at the LabMic (Laboratório Multiusuário de Microscopia de Alta Resolução, Universidade Federal de Goiás, Goiânia, Goiás, Brazil).

The electrochemical measurements consisted of an initial characterization on a three-electrode electrochemical glass cell. The working electrode was fabricated by depositing a previously sonicated catalytic ink, composed of 4 mg of catalyst, dispersed in 4 mL of isopropyl alcohol (Dinâmica, Indaiatuba, SP, Brazil) and 10 μL of a 5 wt.% Nafion® emulsion in a mixture of aliphatic alcohols (Ion Power Inc., Delaware, USA). With the aid of an automatic pipette, 10 μL was deposited on a reticulated vitreous carbon (diameter 5 mm). The counter-electrode was a platinized Pt gauze (Sigma-Aldrich, Jurubatuba, SP, Brazil) of 2 × 2 cm^2, and the reference electrode was a Ag/AgCl electrode (Allum Corp, Orlando, FL, USA). For this initial three-electrode glass cell, the electrolyte used was a 1 mol L^{-1} H_3PO_4 (Sigma-Aldrich, Jurubatuba, SP, Brazil) solution. The sequence of electrochemical measurements consisted of an initial blank voltammetry to estimate the electrochemically active surface area (EASA), followed by the EEO curve in 5 mol L^{-1} ethanol (close to that used in the electroreformer), and finally, a chronoamperometry at 0.5 V *vs*. Ag/AgCl for 30 min. All the three-electrode glass cell measurements were carried out at room temperature. The estimation of the EASA is carried out from the area of the hydrogen desorption peaks after subtraction of the double layer contribution (A_P) from the application of equation 1, where ν is the scan rate, m_{Pt} is the mass of Pt, and Q_H is the integral Faraday charge in the hydrogen desorption region (210 μC cm^{-2} for polycrystalline Pt).[36,37]

$$EASA = \frac{A_P}{\upsilon Q_H m_{Pt}} \quad (1)$$

For the single-cell HT-PA-PBI-PEMEtE, the anodes

with different Pt wt.% were prepared by paint-brushing a catalytic slurry composed of the required mass of catalyst, Nafion® emulsion and a mixture of isopropyl acid and water. The deposited metal loading was 2 mg cm^{-2} of Pt. In the case of the cathodes, a Pt loading of 0.5 mg cm^{-2} was applied from a commercial 20 wt.% Pt/C (Premetek Inc.Cherry Hill, NJ, USA). The electrodes were dried in an oven for 1 h at 80 °C. The PA-PBI membrane (PBI membrane from Blue World Technologies ApS, Aalborg, Denmark) was soaked in 85 wt.% H_3PO_4 for 2 weeks prior to conducting the experiment.

The experimental setup is schematized in Figure S1, Supplementary Information (SI) section. It consisted of an ethanol reservoir containing a mixture of ethanol and water in volumetric ratio of 1:2 (approx. 5.7 mol L^{-1} ethanol). This ratio was selected based on a previous study presented in literature dealing with the optimization of the ethanol concentration.[22] This solution was pumped, with the aid of a peristaltic pump (Exatta Bombas, Palhoça, SC, Brazil), to a vaporizer at a flow rate of 0.5 mL min^{-1}. A former stainless steel granular activated filter was adapted as the vaporizer by being completely wrapped by a heating mantle, and externally isolated to minimize heat losses. The vapor was directed to the ethanol electroreformer, where the cell voltage was linearly swept from open circuit voltage up to 1.0 V, with the aid of a potentiostat/galvanostat PGSTAT302 (Metrohm Autolab BV, Utrecht, the Netherlands) at a scan rate of 0.2 mV s^{-1} (maximum current limited to 1.2 A). The exhaust vapor was sent to a union T-joint, where the capillary of a mass spectrometer (Dymaxion Mass Spectrometer, Ametek, Newark, DE, USA) was coupled to sample the exhaust gases, in order to quantify the products distribution. The chosen mass/charge ratios (*m/z*) were 22 for CO_2 (CO_2^{2+}), 29 for acetaldehyde (CHO^+) (with contributions from ethanol, which were subtracted from the calibration), 31 for ethanol (CH_2OH^+), 60 for acetic acid (CH_3COOH^+) and 61 for ethyl acetate ($CH_3COOH_2^+$). Calibration curves were obtained for each compound to eliminate overlapping contributions, such as ethanol, acetic acid and ethyl acetate on acetaldehyde. The information of each mass was converted, with the aid of the calibration curve, to the maximum corresponding signal (29 for acetaldehyde, 31 for ethanol, 44 for CO_2, 60 for acetic acid and 43 for ethyl acetate). Thereby, it was possible to estimate the product distribution from the relative contribution of each signal, as described by Wang *et al.*[38] The calibration curves are presented in SI section in Figure S2. The rest of the exhaust vapor is condensed and adequately discarded.

Results and Discussion

Table 1 summarizes the main results that can be extracted from the TGA (experimental Pt wt.%), XRD (average crystalline size from the application of the Scherrer's equation)[39] and TEM (average particle size). The information extracted from the TGA analysis and the diffractograms are displayed in Figures S3 and S4 (SI section). As can be observed, the nominal and experimental Pt wt.% of the catalysts are very close, confirming the Pt percentage of the catalysts. On the other hand, all the materials show the typical diffraction peaks associated to Pt(111), Pt(200), Pt(220), Pt(311) and Pt(222) at 39.8, 46.2, 67.5, 81.3 and 85.7 degrees, respectively. As expected, a larger metal content leads to an increase in the average crystalline size, owing to the reduced surface area of the carbon support available for metal dispersion.[40-42] Figure 1 shows the corresponding transmission images of the different catalysts, whereas the particle size distributions are depicted in Figure S5 (SI section). As expected, an increase in the particle size is observed with higher Pt wt.%, as well as a widening of the particle size distribution. The higher metallic loading, combined with the smaller surface area available for Pt anchorage, favors the growth of larger and more heterogeneous particles.

Figure 2 shows the blank voltammetry experiments of the different catalysts. The typical features of Pt nanoparticles can be observed, with hydrogen adsorption/desorption in the low potential region (< 0.15 V *vs*. Ag/AgCl),

Table 1. Average crystalline size from XRD, particle size from TEM and EASA from CV for the different Pt/C catalysts

Theoretical Pt on the carbon support / wt.%	Experimental Pt on the carbon support / wt.%	Average crystalline size from XRD / nm	Average particle size from TEM / nm	EASA / (m^2 g^{-1} of Pt)
20	20.2	3.1	4.0 ± 0.5	41.6 ± 2.9
40	39.2	3.9	4.4 ± 0.5	31.0 ± 3.5
60	59.0	4.6	5.1 ± 0.6	27.6 ± 1.9
80	79.6	5.8	7.5 ± 0.8	19.6 ± 1.5
100 (black)	–	8.4	[a]	12.6 ± 1.0

[a]Not assessed due to the difficulties in counting particles from the micrographies. CV: cyclic voltammetry; wt.%: weight percentage; XRD: X-ray diffraction; TEM: transmission electron micrographies; EASA: electrochemically active surface area.

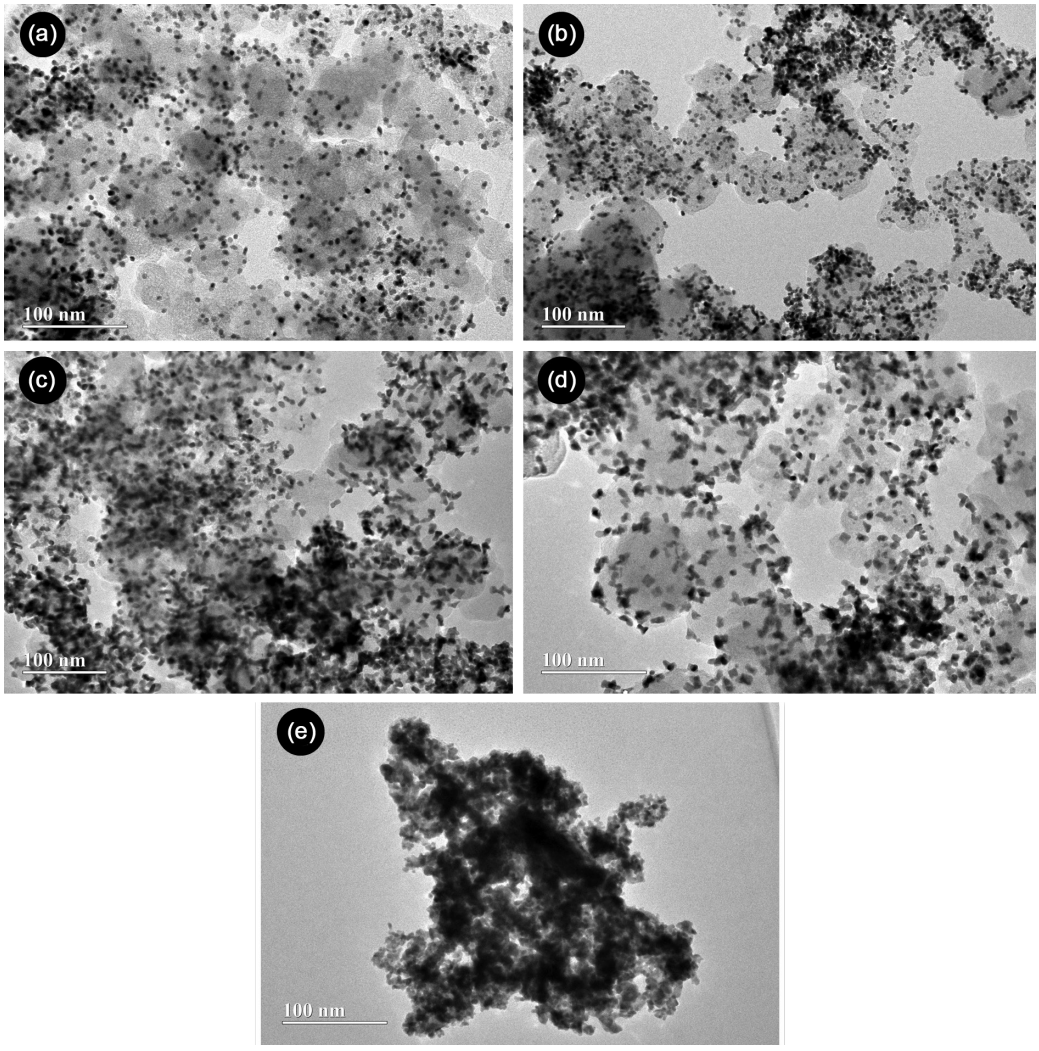

Figure 1. TEM images of the different catalysts: (a) 20 wt.% Pt/C, (b) 40 wt.% Pt/C, (c) 60 wt.% Pt/C, (d) 80 wt.% Pt/C and (e) Pt black.

along with the formation of platinum oxide (PtO) (> 0.55 V *vs*. Ag/AgCl) and the reduction of the formed PtO (backward, maximum ca. 0.5 V *vs*. Ag/AgCl) in the high potential region. One interesting feature is a slight reduction in the PtO reduction peak maximum with increasing Pt wt.% (see dark yellow arrow in the maximum of the PtO reduction peak). Taylor *et al.*[43] observed a similar behavior and related it to the adsorption energy of the oxygenated species onto the Pt surface. Thus, smaller particles adsorb oxygenated species more strongly, resulting in a more oxophilic Pt surface.[44] Such oxygenated species are crucial for the activity of the EEO reaction.[45] The corresponding values of the electrochemical active surface area (EASA) are collected in Table 1, decreasing as expected with increasing Pt content, as a result of the larger Pt nanoparticles observed.

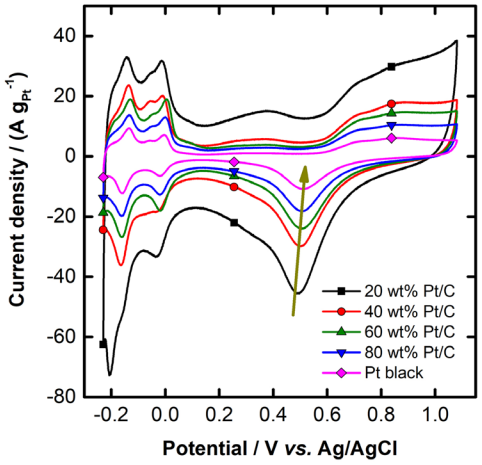

Figure 2. Blank CV of the different catalysts in 1 mol L^{-1} H_3PO_4 (3-electrode glass cell at room temperature).

Figure 3 shows the corresponding forward scans of the EEO voltammetry experiments. The backwards scans are presented and discussed in Figure S4 (SI section). As can be observed in Figure 3a, 20 wt.% Pt/C appears as the most active catalyst in mass terms, as it possesses the smallest particle size and therefore exposes the largest surface area

compared to the other catalysts, which follow the sequence of decreasing activity with higher Pt wt.% values. However, more interesting information can be extracted from the EASA-normalized activity (Figure 3b). Here we can see an increase in the activity up to a metallic wt.% of 60, after which the activity drops (referred to as the maximum current density). In addition, the values of the onset potentials are plotted in the inset of Figure 3b, and follow a slight continuous increase with increasing metallic percentage, especially from 20 to 40 wt.% Pt/C. This onset potential can be explained in terms of the growing oxophilicity of the Pt surface, leading to the formation of the required oxygenated species at lower potentials.[23,46] In the case of the maximum current densities, the largest activity is achieved for the 60 wt.% Pt/C-an intermediate particle size compared to the other catalysts. In the case of the 20 and 40 wt.% Pt/C, the higher oxophilicity, which in principle is beneficial, can limit the performance due to competition from the dissociative adsorption of ethanol (and intermediates) and the poisoning of the Pt surface by oxygenated species, in addition to a stronger adsorption of the intermediates formed.[47,48] Nevertheless, a further decrease in the oxophilicity could be detrimental due to the reduced availability of oxygenated species required for the oxidation of the ethanolic residues formed during the EEO. This, in combination with the smaller active surface area, could be responsible for an early deactivation of the Pt surface and the reduced activity for EEO observed for the 80 wt.% Pt/C and Pt black catalysts.[49] The backward scans also show similar trends (see Figure S6, SI section). Finally, the chronoamperometries (Figure S7, SI section) also show that the best predisposition is achieved using the 60 wt.% Pt/C catalyst for the EEO reaction.

The results of single cell ethanol HT-PA-PBI-PEMEtE are presented in Figure 4. The activity of the Pt/C catalysts follows the following sequence: Pt black << 80% wt.% Pt/C < 20% wt.% Pt/C < 40% wt.% Pt/C < 60% wt.% Pt/C. Considering that all the catalytic layers possess the same Pt mass loading, one might expect a similar trend to that shown in Figure 3a. However, the performance of an electrode in a single-cell device is more complex as other phenomena, such as mass transfer limitations, can play an important role. In this sense, a possible explanation for the different behaviors may lie in the non-negligible mass transfer limitations already observed on HT-PA-PBI DEFC.[22,50] The Pt wt.% values directly impact the thickness of the catalytic layer, whose estimations are collected in Table S1 (SI section). As can be seen, there is a notable decrease in the thickness of the electrode as Pt wt.% increases, which allows more efficient mass transportation. This factor could explain the high performance of the 60 wt.% Pt/C compared to catalysts containing lower metallic percentages, as well as the similar performance of the 80 wt.% Pt/C to the 20 and 40 wt.% Pt/C catalysts, which differ to the results presented in Figure 3a. Finally, Pt black displays the lowest performance as this material possesses the most reduced EASA. Moreover, from a practical point of view, the preparation of Pt black electrodes is not so straightforward, due to the greatly reduced amount of material, which impedes the homogeneous deposition of the catalyst over the diffusion layer.

Figure 5 shows the relative product distribution of the anode exhaust vapor for the different electrocatalysts at 150 and 175 °C. As can be observed, CO_2 percentages of 20-40% are quantified at 150 °C, which further increase to 30-50% at 175 °C, due to the larger amount of available energy, which promotes the kinetics of C–C cleavage.[43,51] In addition, there is a general trend of decreasing CO_2

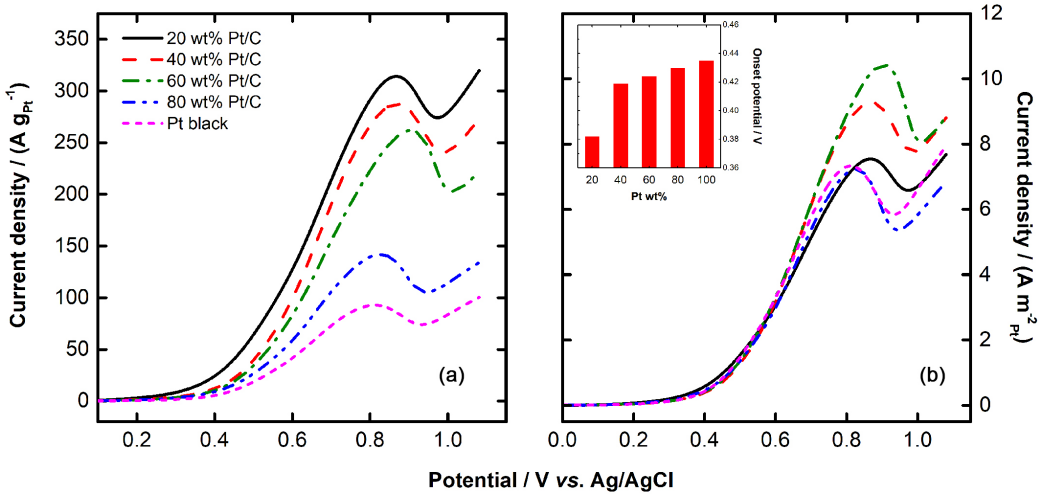

Figure 3. (a) Mass normalized and (b) active area normalized EEO forward scans of the CV curves in 1 mol L^{-1} H_3PO_4 and 5 mol L^{-1} ethanol (inset: onset potential for EEO, 3-electrode glass cell at room temperature).

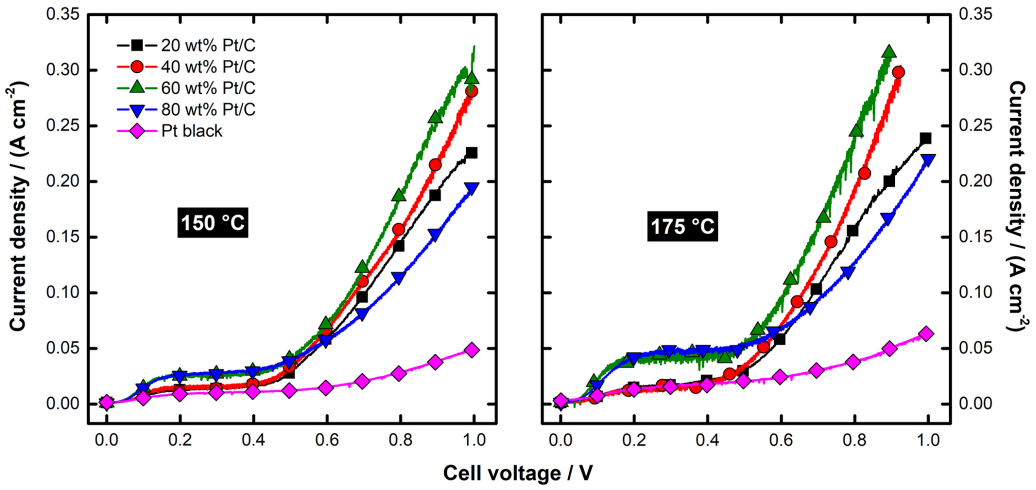

Figure 4. Polarization curves for high temperature ethanol electroreformer at different temperatures (Et:H_2O volume ratio of 1:2 in the fuel).

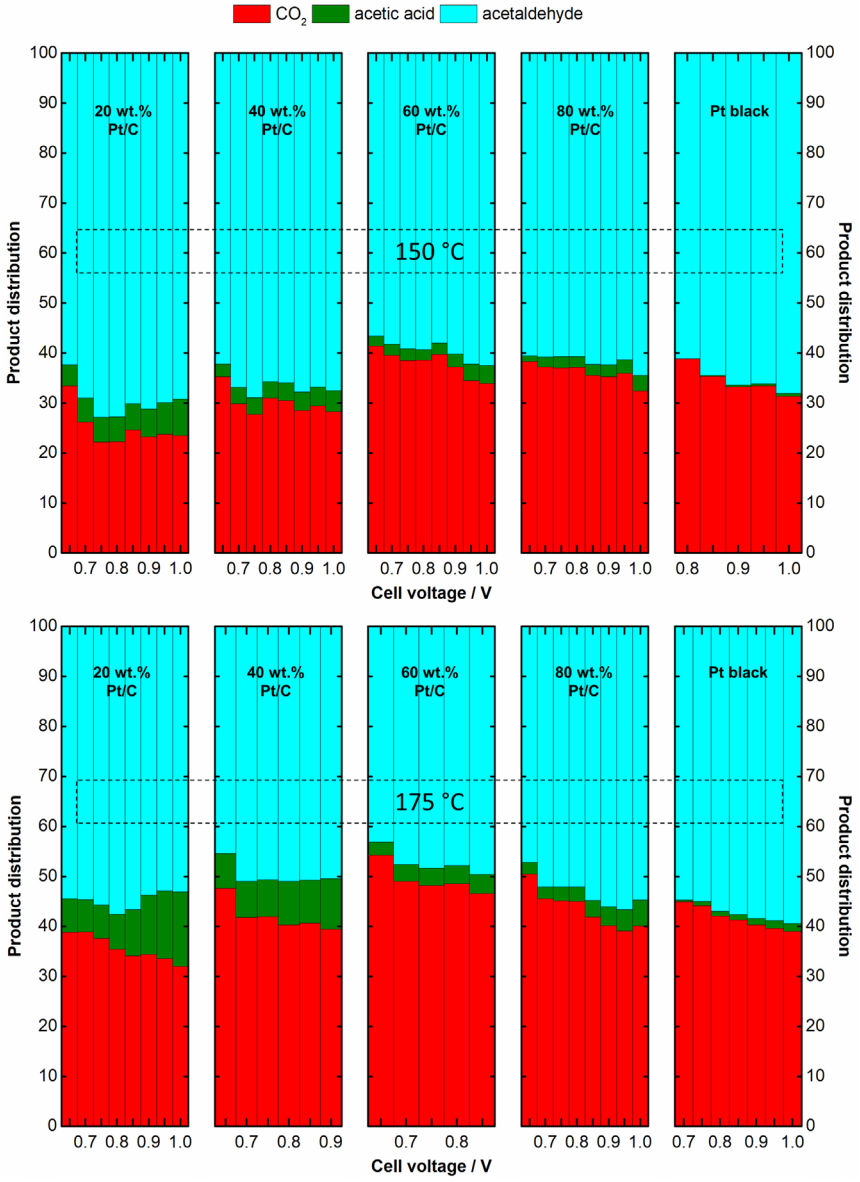

Figure 5. Product distribution for the different catalyst at 150 and 175 °C from the anode exhaust of the ethanol HT-PA-PBI-PEMEtE.

percentage with increasing cell voltage, and a slight increase in the percentage of acetic acid. At higher cell voltages, more oxidized species are expected to cover the Pt surface, which accounts for the increase in the percentage of acetic acid observed. Furthermore, although the formation of CO_2 requires an oxygenated species for oxidizing the $(CH_x)_{ads}$ and CO_{ads} after the C–C cleavage (in the lowest cell voltages where the maximum CO_2 percentage is observed, the low coverage of oxygenated species is still sufficient to allow the oxidation of the C_1 adsorbed species),[52] a large coverage of these species can also reduce the availability of the neighboring Pt active sites necessary for the dissociative adsorption of ethanol. This results in a large percentage of acetaldehyde from the dehydrogenation of the adsorbed ethanol and, to a much lesser extent, acetic acid from the oxidation of the CH_3CO_{ads} with the aid of $–OH_{ads}$ adjacent species.[15,51-57] Regarding the influence of the Pt wt.% in the catalyst formulation, it can be observed that, in overall terms, a maximum CO_2 percentage is achieved using the 60 wt.% Pt/C catalyst. The higher oxophilicity of the 20 and 40 wt.% Pt/C catalysts could be also responsible for the lower CO_2 percentages compared to the 60 wt.% Pt/C catalyst, in which the large coverage of the Pt surface by oxygenated species limits the complete oxidation in favor of incomplete C_2 products (primarily acetaldehyde). However, this trend is not followed for the 80 wt.% Pt/C and Pt black systems. One possible explanation lies in the so-called desorption-re-adsorption-further reaction mechanism applied to EEO by Rao *et al.*[51] and Sun *et al.*[56] (described in detail by Seidel *et al.*):[58] the operation with thick catalytic layers promotes the re-adsorption of the intermediates formed in the EEO reaction (acetaldehyde), which can be further oxidized to CO_2. In the thinner 80 wt.% Pt/C and Pt black catalytic layer, this mechanism is expected to operate to a lesser extent compared to the other Pt wt.%, counterbalancing the effect of reduced Pt poisoning by oxygenated species. In addition, as discussed for the results presented in Figure 5, excessively reduced oxophilicity could also be detrimental, as oxygenated species are required for complete ethanol oxidation.

Figure 6 presents a comparison of the performance of each catalyst at different temperatures in terms of energy demand, hydrogen production and the ratio of H_2 produced to ethanol consumed (this latter parameter directly depends on the product distribution as a result of the definition of the average number of electrons involved in the EEO). The higher this latter parameter, the more efficient the electroreformer. As can be seen, the most favorable performances correspond to the 60 wt.% Pt/C, which produces the maximum amount of H_2 for a fixed energy demand with the highest efficiency (i.e., maximum hydrogen

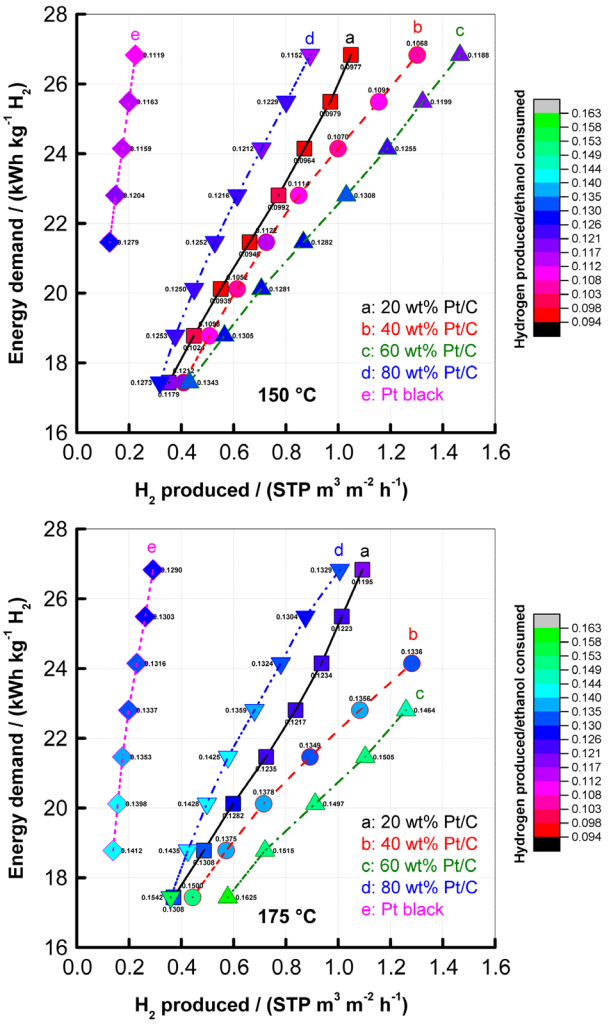

Figure 6. Energy demand, H_2 flux and H_2 production/ethanol consumption (mass base) effiency for the different catalyst at 150 and 175 °C from the date of the HT-PA-PBI-PEMEtE.

production compared to ethanol consumed), as a result of the enhanced capacity to break the C–C bond. In addition, the increase in the temperature slightly increases hydrogen production, as well as the efficiency of H_2 production, due to the enhancement of the performance and the larger CO_2 percentage. In addition, operation at the lowest cell voltages (0.65 and 0.7 V) provides the most efficient conditions for hydrogen production, although the hydrogen flux is reduced. In practical terms, this would imply that a larger electrode area is required for a fixed hydrogen production. This observation shows, in a simplified manner, the complexity of the optimal design and operation of an electroreformer. It follows that engineering and economic studies are required that consider the energy and fuel consumption, the electrode area, as well as the auxiliary system (balance of systems, pump, heat exchangers, etc.).

A brief overview of the previous studies that include the analysis of the product distribution in DEFC and

ethanol electroreformer reveals similar CO_2 percentages (20 to 55%) for HT-PA-PBI-DEFC under similar operating conditions (Pt/C, temperatures, ethanol concentrations and cell voltage/current).[21,31,38] At lower temperatures (< 100 °C, typical range of perfluorinated-based membrane electrolyzers), studies based on the use of Pt/C in DEFC,[51-53,56,59-61] or ethanol electroreformer/electrolyzers,[15,57] have reported CO_2 percentages above 80%. Nevertheless, such high CO_2 yields are attained when the system is operated with ethanol concentrations ≤ 1 mol L^{-1}. Operating with these limited concentrations reduces the capacity for hydrogen production for a determined amount of fuel compared to the more concentrated solutions used in the HT-PA-PBI-PEMEtE. Moreover, the necessity for fuel replenishment would be less frequent, a positive factor for the long-term operation of the electroreformer. Finally, the use of binary PtRu or PtSn for EEO generally leads to a higher EEO activity compared to Pt.[62] Nevertheless, the complete oxidation of ethanol to CO_2 occurs in low percentages, which reduces the efficiency of H_2 production. This, in combination with the use of more dilute ethanol solutions, reduces the potential production of hydrogen from a fixed initial amount of fuel solution. Figure S6 (SI section) graphically summarizes this discussion, displaying the potential hydrogen production efficiency, as well as the available H_2 that could be harvested from the electroreformer as a function of the product distribution and the initial ethanol concentration. Clear advantages can be seen if a catalytic material with high CO_2 conversion is combined with a high H_2 production, as well as a high tolerance to high ethanol concentrations. Figure S7 and Table S2 (SI section) collects a graphic summary of the state-of-the-art of the ethanol electroreforming system in terms of four important parameters: energy demand, H_2 flux, Faradaic efficiency and potential hydrogen production in comparison to this study. As can be seen, the operation of a HT-PA-PBI-PEMEtE allows to increase the Faradaic efficiency of the system as well as it presents the largest potential for hydrogen production due to the possibility of operating with high concentrated ethanol solutions.

Conclusions

In the search for the most active (largest H_2 production) and efficient (maximum CO_2 yield) ethanol electroreformer for green H_2 production, the Pt wt.% plays a key role in maximizing both of these parameters. The sequence of 20-40-60-80 wt.% Pt/C and Pt black catalysts was applied to a HT-PA-PBI-PEMEthE, where temperatures of 150-175 °C were used to intrinsically favor the C–C cleavage to form CO_2. The optimal system was achieved using the intermediate 60 wt.% Pt/C catalyst. Such a Pt wt.% combines a moderate increase in the Pt particle size, and therefore an apparently moderate oxophilicity in the EASA (not so strong as to largely cover and poison the Pt surface, nor so weak as to limit the Pt poisoning by the strongly adsorbed ethanolic residues formed during the EEO) and an optimal catalyst layer thickness (not so thin as to disfavor the re-adsorption process of the acetaldehyde formed), to provide the maximum hydrogen production and the highest CO_2 percentages, thus maximizing the ethanol utilization. The use of this Pt wt.%, in combination with the possibility of feeding the electroreformer with concentrated ethanol solutions, depicts a favorable preliminary scenario for the production of green hydrogen from this type of EtE.

Supplementary Information

Supplementary information (experimental details and complementary results and discussion) is available free of charge at http://jbcs.sbq.org.br as PDF file.

Acknowledgments

The authors would like to thank Fundação de Apoio à Pesquisa do Distrito Federal (FAPDF, process No. 0193.001.473/2017) for the financial support and FINEP through the DENDEPALM project.

References

1. Falcone, P. M.; Hiete, M.; Sapio, A.; *Curr. Opin. Green Sustainable Chem.* **2021**, *31*, 100506. [Crossref]
2. Chai, S.; Zhang, G.; Li, G.; Zhang, Y.; *Clean Technol. Environ. Policy* **2021**, *23*, 1931. [Crossref]
3. Chisholm, G.; Cronin, L. In *Storing Energy*; Letcher, T. M., ed.; Elsevier: Amsterdam, The Netherlands, 2016, p. 315-343. [Crossref]
4. Pyun, S.-I.; *J. Solid State Electrochem.* **2020**, *24*, 2165. [Crossref]
5. International Renewable Energy Agency (IRENA); *Green Hydrogen Cost Reduction: Scaling up Electrolysers to Meet the 1.5 ºC Climate Goal*; 2020. https://irena.org/-/media/Files/IRENA/Agency/Publication/2020/Dec/IRENA_Green_hydrogen_cost_2020.pdf, accessed in April 2022
6. Trocino, S.; Lo Vecchio, C.; Campagna Zignani, S.; Carbone, A.; Saccà, A.; Baglio, V.; Gómez, R.; Aricò, A. S.; *Catalysts* **2020**, *10*, 1319. [Crossref]
7. Linares, J. J.; Vieira, C. C.; Costa Santos, J. B.; Magalhães, M. M.; dos Santos, J. R. N.; Carvalho, L. L.; dos Reis, R. G.

C. S.; Colmati, F. In *Electrochemical Methods for Hydrogen Production*; Scott, K., ed.; Royal Society of Chemistry: Croydon, UK, 2019, p. 94-135. [Crossref]

8. Arshad, F.; Haq, T. ul; Hussain, I.; Sher, F.; *ACS Appl. Energy Mater.* **2021**, *4*, 8685. [Crossref]
9. Gutiérrez-Martín, F.; Calcerrada, A. B.; de Lucas-Consuegra, A.; Dorado, F.; *Renewable Energy* **2020**, *147*, 639. [Crossref]
10. Ruiz-López, E.; Amores, E.; Raquel de la Osa, A.; Dorado, F.; de Lucas-Consuegra, A.; *Chem. Eng. J.* **2020**, *379*, 122289. [Crossref]
11. Ying, Z.; Geng, Z.; Zheng, X.; Dou, B.; Cui, G.; *Int. J. Hydrogen Energy* **2021**, *46*, 119. [Crossref]
12. Jahromi, A. F.; Ruiz-López, E.; Dorado, F.; Baranova, E. A.; de Lucas-Consuegra, A.; *Renewable Energy* **2022**, *183*, 515. [Crossref]
13. Palanisamy, A.; Soundarrajan, N.; Ramasamy, G.; *Environ. Sci. Pollut. Res.* **2021**, *28*, 63690. [Crossref]
14. Luo, H.; Barrio, J.; Sunny, N.; Li, A.; Steier, L.; Shah, N.; Stephens, I. E. L.; Titirici, M.; *Adv. Energy Mater.* **2021**, *11*, 2101180. [Crossref]
15. Altarawneh, R. M.; Pickup, P. G.; *J. Electrochem. Soc.* **2017**, *164*, F861. [Crossref]
16. Kavanagh, R.; Cao, X.-M.; Lin, W.-F.; Hardacre, C.; Hu, P.; *Angew. Chem., Int. Ed.* **2012**, *51*, 1572. [Crossref]
17. Soares, L. A.; Morais, C.; Napporn, T. W.; Kokoh, K. B.; Olivi, P.; *J. Power Sources* **2016**, *315*, 47. [Crossref]
18. Beyhan, S.; Coutanceau, C.; Léger, J.-M.; Napporn, T. W.; Kadırgan, F.; *Int. J. Hydrogen Energy* **2013**, *38*, 6830. [Crossref]
19. Wnuk, P.; Jurczakowski, R.; Lewera, A.; *Electrocatalysis* **2020**, *11*, 121. [Crossref]
20. Jin, J.-M.; Sheng, T.; Lin, X.; Kavanagh, R.; Hamer, P.; Hu, P.; Hardacre, C.; Martinez-Bonastre, A.; Sharman, J.; Thompsett, D.; Lin, W.-F.; *Phys. Chem. Chem. Phys.* **2014**, *16*, 9432. [Crossref]
21. Linares, J. J.; Zignani, S. C.; Rocha, T. A.; Gonzalez, E. R.; *J. Appl. Electrochem.* **2013**, *43*, 147. [Crossref]
22. Lobato, J.; Cañizares, P.; Rodrigo, M. A.; Linares, J. J.; *Fuel Cells* **2009**, *9*, 597. [Crossref]
23. Perez, J.; Paganin, V. A.; Antolini, E.; *J. Electroanal. Chem.* **2011**, *654*, 108. [Crossref]
24. Singh, S.; Datta, J.; *Ionics* **2011**, *17*, 785. [Crossref]
25. Lamy, C.; Jaubert, T.; Baranton, S.; Coutanceau, C.; *J. Power Sources* **2014**, *245*, 927. [Crossref]
26. Qi, J.; Jiang, L.; Jing, M.; Tang, Q.; Sun, G.; *Int. J. Hydrogen Energy* **2011**, *36*, 10490. [Crossref]
27. Frota Jr., E. F.; de Barros, V. V. S.; de Araújo, B. R. S.; Purgatto, Â. G.; Linares, J. J.; *Int. J. Hydrogen Energy* **2017**, *42*, 23095. [Crossref]
28. Fan, S.; Wilkinson, D. P.; Wang, H.; *J. Electrochem. Soc.* **2012**, *159*, B570. [Crossref]
29. Camargo, A. P. M.; Previdello, B. A. F.; Varela, H.; Gonzalez, E. R.; *Quim. Nova* **2010**, *33*, 2143. [Crossref]
30. Camargo, A. P. M.; Previdello, B. A. F.; Varela, H.; Gonzalez, E. R.; *Electrochem. Commun.* **2010**, *12*, 140. [Crossref]
31. Linares, J. J.; Rocha, T. A.; Zignani, S.; Paganin, V. A.; Gonzalez, E. R.; *Int. J. Hydrogen Energy* **2013**, *38*, 620. [Crossref]
32. Lobato, J.; Cañizares, P.; Ubeda, D.; Pinar, F. J.; Rodrigo, M. A.; *Appl. Catal., B* **2011**, *106*, 174. [Crossref]
33. López-Rosas, D. M.; Félix-Navarro, R. M.; Flores-Hernández, J. R.; Silva-Carrillo, C.; Albarrán-Sánchez, I. L.; Reynoso-Soto, E. A.; *J. Mex. Chem. Soc.* **2021**, *65*, 39. [Crossref]
34. Liu, B.; Creager, S.; *J. Power Sources* **2010**, *195*, 1812. [Crossref]
35. Jung, J.-H.; Cha, M.-S.; Kim, J.-B.; *J. Nanosci. Nanotechnol.* **2012**, *12*, 5412. [Crossref]
36. Xia, Y.-F.; Guo, P.; Li, J.-Z.; Zhao, L.; Sui, X.-L.; Wang, Y.; Wang, Z.-B.; *iScience* **2021**, *24*, 103024. [Crossref]
37. Rheinländer, P. J.; Herranz, J.; Durst, J.; Gasteiger, H. A.; *J. Electrochem. Soc.* **2014**, *161*, F1448. [Crossref]
38. Wang, J.; Wasmus, S.; Savinell, R. F.; *J. Electrochem. Soc.* **1995**, *142*, 4218. [Crossref]
39. Patterson, A. L.; *Phys. Rev.* **1939**, *56*, 978. [Crossref]
40. Kholodovich, A. N.; Simonov, P. A.; *React. Kinet. Catal. Lett.* **2005**, *86*, 381. [Crossref]
41. Álvarez-Montero, M. A.; Rodriguez, J. J.; Gómez-Sainero, L. M.; *Nanomater. Nanotechnol.* **2016**, *6*, 18. [Crossref]
42. Shin, J. H.; Kwon, D. W.; Kim, G. J.; Hong, S. C.; *Appl. Chem. Eng.* **2018**, *29*, 22. [Crossref]
43. Taylor, S.; Fabbri, E.; Levecque, P.; Schmidt, T. J.; Conrad, O.; *Electrocatalysis* **2016**, *7*, 287. [Crossref]
44. Takasu, Y.; Ohashi, N.; Zhang, X.-G.; Murakami, Y.; Minagawa, H.; Sato, S.; Yahikozawa, K.; *Electrochim. Acta* **1996**, *41*, 2595. [Crossref]
45. Yaqoob, L.; Noor, T.; Iqbal, N.; *RSC Adv.* **2021**, *11*, 16768. [Crossref]
46. Frelink, T.; Visscher, W.; van Veen, J. A. R. A. R.; *J. Electroanal. Chem.* **1995**, *382*, 65. [Crossref]
47. Mukerjee, S.; McBreen, J.; *J. Electroanal. Chem.* **1998**, *448*, 163. [Crossref]
48. Li, X.; Qiu, X.; Yuan, H.; Chen, L.; Zhu, W.; *J. Power Sources* **2008**, *184*, 353. [Crossref]
49. Tang, Y.; Zhang, L.; Wang, Y.; Zhou, Y.; Gao, Y.; Liu, C.; Xing, W.; Lu, T.; *J. Power Sources* **2006**, *162*, 124. [Crossref]
50. Lobato, J.; Cañizares, P.; Rodrigo, M. A.; Linares, J. J.; Úbeda, D.; Pinar, F. J.; *Fuel Cells* **2010**, *10*, 312. [Crossref]
51. Rao, V.; Cremers, C.; Stimming, U.; Cao, L.; Sun, S.; Yan, S.; Sun, G.; Xin, Q.; *J. Electrochem. Soc.* **2007**, *154*, B1138. [Crossref]
52. Seweryn, J.; Lewera, A.; *Appl. Catal., B* **2014**, *144*, 129. [Crossref]

53. Wnuk, P.; Lewera, A.; *Electrochim. Acta* **2020**, *330*, 135256. [Crossref]
54. Altarawneh, R. M.; Pickup, P. G.; *J. Power Sources* **2017**, *366*, 27. [Crossref]
55. Gomes, J. F.; Bergamaski, K.; Pinto, M. F. S. S.; Miranda, P. B.; *J. Catal.* **2013**, *302*, 67. [Crossref]
56. Sun, S.; Halseid, M. C.; Heinen, M.; Jusys, Z.; Behm, R. J.; *J. Power Sources* **2009**, *190*, 2. [Crossref]
57. Altarawneh, R. M.; Majidi, P.; Pickup, P. G.; *J. Power Sources* **2017**, *351*, 106. [Crossref]
58. Seidel, Y. E.; Schneider, A.; Jusys, Z.; Wickman, B.; Kasemo, B.; Behm, R. J.; *Faraday Discuss.* **2009**, *140*, 167. [Crossref]
59. Nakagawa, N.; Kaneda, Y.; Wagatsuma, M.; Tsujiguchi, T.; *J. Power Sources* **2012**, *199*, 103. [Crossref]
60. James, D. D.; Bennett, D. V.; Li, G.; Ghumman, A.; Helleur, R. J.; Pickup, P. G.; *Electrochem. Commun.* **2009**, *11*, 1877. [Crossref]
61. Rousseau, S.; Coutanceau, C.; Lamy, C.; Léger, J.-M.; *J. Power Sources* **2006**, *158*, 18. [Crossref]
62. Wala, M.; Simka, W.; *Molecules* **2021**, *26*, 2144. [Crossref]

Submitted: January 13, 2022
Published online: April 19, 2022